Atmos. Meas. Tech. Discuss., 6, 2501–2531, 2013
www.atmos-meas-tech-discuss.net/6/2501/2013/
doi:10.5194/amtd-6-2501-2013

Atmospheric Measurement Techniques Discussions

Mid-upper tropospheric methane retrieval from IASI and its validation

X. Xiong[1,2], **C. Barnet**[2], **E. S. Maddy**[3,2], **A. Gambacorta**[1,2], **T. S. King**[1,2], **and S. C. Wofsy**[4]

[1]I. M. Systems Group, Rockville, MD 20852, USA
[2]National Environmental Satellite, Data, and Information Service, NOAA, USA
[3]Science and Technology Corporation, Langley, VA, USA
[4]Department of Earth and Planetary Sciences, Harvard University, Cambridge, MA, USA

Received: 31 December 2012 – Accepted: 28 February 2013 – Published: 11 March 2013

Correspondence to: X. Xiong (xiaozhen.xiong@noaa.gov)

Published by Copernicus Publications on behalf of the European Geosciences Union.

Abstract

Mid-upper tropospheric atmospheric methane (CH_4), as an operational product at NOAA's (National Oceanic and Atmospheric Administration) Comprehensive Large Array-data Stewardship System (CLASS), has been retrieved from the Infrared Atmospheric Sounding Interferometer (IASI) since 2008. This paper provides a description of the retrieval method and the validation using 596 CH_4 vertical profiles from aircraft measurements by the HIAPER Pole-to-Pole Observations (HIPPO) program over the Pacific Ocean. The degree of freedom of the CH_4 retrieval is mostly less than 1.5, and it decreases under cloudy conditions. The most sensitivity layer is between 100–600 hPa in the tropics, 200–750 hPa in the mid to high latitude. Validation is accomplished using aircraft measurements (convolved by applying the averaging kernels) collocated with all the retrieved profiles within 200 km and in the same day, and the results show that, on average, the largest error of CH_4 occurs at 300–500 hPa, and the bias in the trapezoid of 374–477 hPa is −1.74 % with residual standard deviation of 1.20 %. The retrieval error is relatively larger in the high northern latitude regions and/or under cloudy conditions. The main reasons for this negative bias might be due to the uncertainty in the spectroscopy near methane Q-branch and/or the empirical bias correction, plus cloud-contamination in the cloud-cleared radiances. It is expected for NOAA to generate the CH_4 product for 20+ yr using similar algorithm from three similar thermal infrared sensors, i.e. Atmospheric Infrared Sounder (AIRS), IASI and the Cross-track Infrared Sounder (CrIS). Such a unique product will provide a supplementary to current ground-based observation network, particularly in the Arctic, for monitoring the CH_4 cycle, its transport and trend associated with climate change.

1 Introduction

As one of the most important greenhouse gases after carbon dioxide (CO_2), atmospheric methane (CH_4) is 25 times more effective on a per unit mass basis than carbon

AMTD
6, 2501–2531, 2013

dioxide in absorbing long-wave radiation on a 100-yr time horizon, and accounts for 18 % of the total of 2.66 $W m^{-2}$ of the anthropogenically produced greenhouse gas radiative forcing (IPCC, 2007). It also plays an important role in atmospheric ozone chemistry (e.g. in the presence of nitrogen oxides, tropospheric methane oxidation will lead to the formation of ozone) and in enriching moisture in the stratosphere (e.g. Brasseur et al., 1998). The concentration of CH_4 in the atmosphere has increased from the pre-industrial levels of about 700 ppb (parts per billion) to about 1800 ppb. However, it experienced a nearly stable period of about one decade (e.g. Dlugokencky et al., 2003; Simpson et al., 2002) before a renewed increase was found in 2007 and the following years (Rigby et al., 2008; Dlugokencky et al., 2009; Sussmann et al., 2012). While the recent increase of CH_4 in 2007–2008 is more likely attributed to the increased emissions from tropical and Arctic wetlands (Rigby et al., 2008; Dlugokencky et al., 2009), the uncertainty still exists, and one major concern is the amount of CH_4 release from permafrost soils and continental shelves, a likely positive feedback of Arctic warming (Walter et al., 2006; Zimov et al., 2006; MacDougall et al., 2008; Shakhova et al., 2010, 2011; Biastoch et al., 2011; Kort et al., 2012).

The primary data used as a constraint for model simulation to quantify the global CH4 sources and sinks is still high-precision in-situ measurements of CH_4 mixing ratios (e.g. Chen and Prinn, 2006; Bousquet et al., 2006, 2011) and the CH_4 isotopes, and these data have been acquired at the sites of NOAA/ESRL/GMD (National Oceanic and Atmospheric Administration, Earth System Research Laboratory, Global Monitoring Division) networks and some other sites under the umbrella of the Global WMO (World Meteorological Organization) Atmosphere Watch (GAW) programme for more than 25 yr. However, quantification of different emission source types and source regions still has large uncertainties, due to a large spatial and temporal variation of different CH_4 emission sources and the sparse sites of ground observational network, particularly in the polar regions (Zhuang et al., 2009). Recent satellite observations provide the measurement of CH_4 with a large spatial and temporal coverage, and they can be used as an additional constraint for inverse modeling (e.g. Wecht et al., 2012).

AMTD
6, 2501–2531, 2013

Space-borne measurements of CH_4 include the use of the thermal infrared (TIR) sounders (with their most sensitivity to the mid-upper tropospheric CH_4), the near-IR(NIR) measurements (with sensitivity to the total column amount of CH_4), and the limb sounding (with sensitivity to CH_4 in the upper troposphere and stratosphere). The TIR observations of CH_4 profile include the Interferometric Monitor for Greenhouse Gases (IMG) onboard the Advanced Earth Observing Satellite (ADEOS) (Clerbaux et al., 2003), the Tropospheric Emission Spectrometer (TES) on NASA/Aura (Payne et al., 2009; Wecht et al., 2012; Worden et al., 2012), the AIRS on NASA/AQUA (Aumann et al., 2003; Xiong et al., 2008, 2009, 2010a,b), and the IASI on METEOP-A (Crevoisier et al., 2009; Razavi et al., 2009). The NIR observations of CH_4 total column include the SCanning Imaging Absorption spectroMeter for Atmospheric CHartographY (SCIAMACHY) instrument onboard ENVISAT for 2003–2009 (e.g. Frankenberg et al., 2008, 2011), and the Greenhouse gases Observation SATellite (GOSAT) from 2009–present, which also carries the TIR observation (Yokota et al., 2008; Schepers et al., 2012). Space-borne observations working in a limb geometry include ACE-FTS (e.g. De Maziere et al., 2008), HALOE (e.g. Park et al., 2004) and MIPAS (e.g. Payan et al., 2007).

Retrievals of CH_4 from IASI have been successfully made before (for example, Crevoisier et al., 2009; Razavi et al., 2009), but their algorithms are different from that used in NOAA system and the data from either of them have not been fully validated. Crevoisier et al. (2009) reported their first year retrieval results in clear sky and tropical ocean condition based on neural networks. Nine strong CH_4 absorption channels in 1301–1305 cm^{-1} were used. Razavi et al. (2009) reported some characteristics of methane retrievals based on the Optimal Estimation Method (Rodgers, 2000) and used channels in the spectral range from 1240–1290 cm^{-1} (the channels in the Q branch located near 1306 cm^{-1} were avoided). Using an algorithm similar to that in AIRS-V5 (Xiong et al., 2008), NOAA has been generating the CH_4 profile using IASI data since 2008. Due to the uncertainties in the satellite remote sensing resulted from many factors involved with the radiative transfer modeling in the atmosphere–Earth system, and

AMTD
6, 2501–2531, 2013

observational noise, validation to the IASI CH_4 profile through comparison with aircraft measurements is vital for the users to understand the uncertainties of this product, so as to better use this product in their researches. Therefore, in this study we validate the NOAA IASI CH_4 product using HIPPO aircraft measurements data in all 5 campaigns. Section 2 gives a brief introduction of the IASI instrument, retrieval methodology and some characteristics of the retrieval product. Section 3 describes the aircraft measurements data, the mechanics of validation by applying the averaging kernels, and the detail validation results. A summary and discussion are given in Sect. 4.

2 The IASI instrument and the methane retrieval

2.1 Description of IASI instrument and the NOAA retrieval system

The IASI is a cross-track-scanning Michelson interferometer that measures 8461 channels at 0.25 cm^{-1} spacing in three bands between 645 to 2760 cm^{-1} in a 2 × 2 array of circular footprints with a nadir spatial resolution of roughly 50 km × 50 km (with a corresponding single footprint spatial resolution at nadir of roughly 12 km). IASI on Metop-A platform was launched into a 817-km-altitude polar orbit on 19 October 2006, and Metop-B was launched on 17 September 2012. The satellite crosses the equator at approximately 09:30 and 09:30 LT (local time), resulting in near global coverage twice a day. The on-flight Noise Equivalent Delta Temperature (NEDT) at 280 K has been estimated to be well below 0.1 K in the spectral range of methane (Razavi et al., 2009). Like AIRS, IASI has a wide swath with the scan angle ±48.3°. Its nominal scan line covers 30 scan positions towards the Earth with four instantaneous field of view (IFOV). The Advanced Microwave Sounding Unit (AMSU) is also flying together with IASI, and in NOAA retrieval system both IASI and AMSU are used in order to make retrieval in clear and partial cloudy conditions (Maddy et al., 2011, 2012). IASI level1c and AMSU Level1b data are available since July 2007.

AMTD
6, 2501–2531, 2013

The IASI retrieval system at NOAA/NESDIS was built to emulate the AIRS-V5 retrieval system, and has been put into operation at NOAA's CLASS since 2008 (Maddy et al., 2009). More detail about the AIRS retrieval system (V5) can be referred to Susskind et al. (2003) and the references therein. The NOAA IASI retrieval system is a sequential retrieval using both IASI and AMSU observations, including the steps of microwave only retrieval, cloud clearing, initial IR retrieval, and a final physical retrieval. The CH_4 retrieval is performed on basis of successful retrievals of water vapor profile, temperature profile and surface characteristics, and can work on clear and partially cloudy conditions. Under partially cloudy conditions, we used the cloud-cleared radiance which was derived by using 4 IASI FOV contained in each single AMSU FOV for removing the effect of clouds on the IASI observed infrared radiance. The retrievals are performed with a nadir spatial resolution of about 45 km. These products, including CH_4, are currently available at the NOAA CLASS (http://www.nsof.class.noaa.gov/saa/products/search?datatype_family=IASI).

2.2 Retrieval method and its optimization

Similar to the AIRS CH_4 retrieval (Xiong et al., 2008), channels in the whole CH_4 absorption band near 7.66 μm that are sensitive to CH_4 but insensitive to N_2O and HNO_3 were selected. In the NOAA IASI retrieval system (V2), 60 IASI channels were selected, and they include both the strong CH_4 channels near the CH_4 Q branch, which are more sensitive to CH_4 in the upper troposphere, as well as channels near 1230 cm^{-1} that are sensitive to the lower troposphere (Worden et al, 2012). Figure 1 shows one example of the observed IASI radiance and the channels used in the retrieval (red triangle). In the CH_4 retrieval, the atmospheric temperature profile, water profile, surface temperature and surface emissivity are required as inputs, and these variables are derived from other separate IASI channels. To input these data and the CH_4 first-guess profile to the forward model (Strow et al., 2003), we can get the computed upwelling radiance.

AMTD
6, 2501–2531, 2013

The difference between the computed radiance and the cloud cleared radiance, ΔR, is used to compute a change to the CH_4 profile, Δx, as follows:

$$\Delta R_n = S_{n,L} \cdot \Delta X_L + \varepsilon \quad (1)$$

where R_n is the cloud cleared radiance (observed), and ΔR_n is R_n minus the calculated radiance in channel n, $S_{n,L}$ is the sensitivity of radiance in channel n to the change of CH_4 for layer L, and ΔX_L is the difference of CH_4 from the first-guess at layer L that needs to be derived. Equation (1) can be solved using singular value decomposition (SVD) of the covariance matrix of the sensitivity weighted by an inverse of the estimates of the precision and accuracy of our radiative transfer model and the errors and noise in the measurements. Damping the least significant eigenfunctions of the SVD to constrain the solution, the change in CH_4 can be written as:

$$\Delta X_L = \boldsymbol{U} \cdot \frac{1}{\lambda + \Delta\lambda} \cdot U^T \cdot S^T \cdot \mathbf{W} \cdot (\Delta R_n - \Phi_n) \quad (2)$$

where $\boldsymbol{U}$ is the eigenvector from the SVD, $\mathbf{W}$ is an inverse matrix of the error that represents the weight based on the estimated precision and accuracy of our radiative transfer model and the errors and noise in the measurements, Φ_n is background term (Susskind et al., 2003), and ^{T} represent the transpose operator. $\Delta\lambda$ is the damping variable proportional to the eigenvalue λ as defined in Eq. (4) of Maddy and Barnet (2008) and Eq. (3) of McMillan et al. (2011). This retrieval methodology minimizes the dependence of the solution to the a priori first-guess profile and covariance matrix, and relies exclusively on the signal to noise of the observation. The eigenvalues, λ, give an indication of the usefulness of each component and are used to determine the damping variable in the retrieval. A more detailed description of this algorithm is found in Susskind et al. (2003) and Xiong et al. (2008).

As the information content of the IASI CH_4 channels near 7.66 μm is redundant and the largest sensitivities of these channels to CH_4 are mostly limited in a broad layer near the mid to upper troposphere, so in the IASI CH_4 retrieval 11 layers (Table 1) that are set as a series of 11 vertically overlapping trapezoidal functions are used (Fig. 2).

AMTD
6, 2501–2531, 2013

The CH_4 first guess profile ("a priori"), as described in Xiong et al. (2008), is given as a smoothed function of latitude and pressure (to capture its strong latitudinal and vertical gradients), and no temporal and longitudinal variation are introduced in the retrieval. Figure 3 shows the examples of the first guess profiles in 5 different latitudes (60° S, 30° S, 0, 30° N and 60° N).

2.3 Averaging kernels and the retrieval sensitivity

The averaging kernels are defined to provide a simple characterization of the relationship between the retrieval and true state. The retrieval sensitivity can be seen from the sum of each column of averaging kernel matrix, which is also referred to as "the area of the averaging kernel" (Rodgers, 2000). More detail about the computation of averaging kernels can be referred to Maddy and Barnet (2008) and Xiong et al. (2008). As an example, Fig. 4 shows the averaging kernels in the high northern latitude and in the tropics in September 2009. It is evident that the averaging kernels corresponding to 11 different trapezoidal functions are broad and exhibit significant overlap, indicating that the retrieved amounts of CH_4 at different layers are not independent. The degree of freedom (DOF), defined as the fractional number of significant eigenfunctions used in the retrieval process and computed as the trace of the averaging kernel matrix, is about 1.28 in the tropics and 0.98 in the HNH in this case. In general, the DOF in the tropic is higher than in the high latitudes, and in the summer is higher than in winter.

To better see the retrieval sensitivity in different latitudes, Fig. 5 plots the the color map of the area of the averaging kernels in different latitudes. From Fig. 5 we can see that the peak sensitivity near the tropics is between 100–600 hPa, while in the mid-high latitude regions, the peak sensitivity is between 200–750 hPa. Due to the impact of the temperature and moisture profiles, the vertical sensitivity of the retrieval has large geographic and seasonal variability.

AMTD
6, 2501–2531, 2013

2.4 Setting of quality flag

To make sure a stable retrieval result is used in the validation and future data analysis, we noticed that it is necessary to set an appropriate quality control. From the experiences we learned, the retrieved profile meeting the following criteria is the one with good quality and recommended for use:

1. Both infrared and microwave retrievals of water vapor and temperature are successful;

2. Residual (observation minus RTA computation) relative to the estimated errors (including error in instrument, cloud-clearing, forward model), χ^2, is less than 3 ($\chi^2 < 3$). The χ^2 is computed as below. N is the total number of channels used for CH_4 retrieval, and $W_{n,n}$ represents the entry on the ith row and i-th column of matrix **W**.

$$\chi^2 = \left\{ \left[\sum_{n=1}^{N} (\Delta R_n \cdot \Delta R_n)/W_{n,n} \right] /N \right\}^{1/2} \quad (3)$$

3. Total FOR Cloud fraction, solving for two layers of clouds, is less than 1.5;

4. DOF is greater than 0.4.

3 Validation

3.1 Data of aircraft measurement of CH_4 profile from HIPPO -1, -2, -3, -4, -5

Aircraft measurements of the CH_4 vertical profiles by the HIAPER Pole-to-Pole Observations (HIPPO) program over the Pacific Ocean (Wofsy et al., 2011) provide a unique dataset for validation over a wide latitudinal range (67° S – 85° N). Figure 6 shows the

AMTD
6, 2501–2531, 2013

flight paths of NSF's Gulfstream V (GV) during all the five HIPPO missions in January 2009 (HIPPO 1), October–November 2009 (HIPPO 2), May–April 2010 (HIPPO 3), June–July 2011(HIPPO-4) and August–September 2011 (HIPPO-5), with the location of the selected aircraft measurements. The GV transected the Pacific Ocean from 85° N to 67° S, performing in-progress vertical profiles every 220 km or 20 min (Wofsy et al., 2011). CH_4 was measured with a Quantum Cascade Laser Spectrometer (QCLS) at 1 Hz frequency with accuracy of 1.0 ppb and precision of 0.5 ppb (Kort et al., 2011). HIPPO methane data are reported on the NOAA04 calibration scale. The NOAA04 scale was designated as the official calibration scale, and consists of 16 gravimetrically prepared primary standards covering the nominal range of 300 to 2600 nmol mol^{-1}. This makes it suitable for use in calibrating standards for the measurement of air extracted from ice cores and contemporary measurements from GAW sites. This new scale results in CH_4 mole fractions that are a factor of 1.0124 greater than the previous scale (now designated CMDL83) (Dlugokencky et al., 2005). We isolated each vertical profile performed by the GV based on the flight distance and height.

Similar to TES validation (Wecht et al., 2012), for each HIPPO vertical profile (covering 220 km in 20 min), we calculated the mean location (latitude and longitude) and time. All IASI retrievals coincident with each HIPPO profile in a collocation window with a distance of 200 km and in the same day and passing the quality control check were used to compute the mean profile, which is then compared to the corresponding HIPPO aircraft profile after applying the averaging kernels, as described later.

3.2 Mechanics of validation

In order to take into account the skill of the CH_4 retrievals, the averaging kernels need to be applied to the in situ aircraft data for validating the retrieved profile from IASI. This can be done based on the following equation:

$$\hat{x} = \mathbf{A}x + (\mathbf{I} - \mathbf{A})x_a \quad (4)$$

AMTD
6, 2501–2531, 2013

where **A** is the identity matrix, **A** is the averaging kernel matrix, x_a is the first guess profile, x is the in situ aircraft measurement profile, and the computed value of $\hat{x}$ is referred to as the convolved data later in this paper and will be compared with the retrieved CH_4 mixing ratio. Note we need to take log to x, x_a, $\hat{x}$ when applying the averaging kernels (see Xiong et al., 2008).

As the aircraft profiles do not span the entire vertical range defined by the IASI averaging kernels, extension of the aircraft profiles is required, and usually this can be done using output from a chemistry model or climatology to represent the upper troposphere and higher levels. In this paper we used the monthly averaged CH_4 data from 2007 from an Atmospheric General Circulation Model (AGCM)-based chemistry transport model (hereinafter ACTM) (Patra et al., 2011) to extrapolate from the ceiling of the aircraft profile to the top of atmosphere and from the lowest measurement height to the bottom of the atmosphere. The profile is then mapped to the 100 levels grid of RTA (Strow et al., 2003). The HIPPO aircraft profiles with their ceilings lower than 350 hPa were not used.

As the averaging kernels are not outputs in the NOAA CLASS, we used the monthly mean averaging kernels that were generated from our run in local machine and saved as 3×3 degree grid product. The averaging kernels in the closest grid point to the in situ observation are selected to convert the corresponding the aircraft profile. The averaging kernels matrix (11×11) is also mapped to 100×100 (Maddy and Barnet, 2008), so the retrieve profiles and the convolved data can be compared at the 100 level grid of RTA and the coarse layers of the trapezoid functions.

4 Results

As an example to illustrate the validation procedure, Fig. 7 shows the comparison of one HIPPO measurement in the mid-latitude in 30 March 2010 with all accepted IASI retrievals in a collocation window with a distance of 200 km and in the same day. Comparison of the mean IASI retrieved profile with the profile from aircraft measurements

AMTD
6, 2501–2531, 2013

(both the convolved and non-convolved with the averaging kernels are shown) indicates that they are in a good agreement, except the retrieved profile is smoother and cannot capture the fine vertical structure seen in aircraft measurements, for example near 450 and 750 hPa. This is understandable as the retrieved profile at each layer represents a weighted average of the real profile in its surrounding a few layers, thus it smoothes out some fine vertical structure. Compared to the first guess (dash-line), IASI retrieved mean profile is closer to the in-situ aircraft observation at its sensitive layer between 300–750 hPa.

Statistics analysis of the validation results using all 596 profiles from five campaigns of HIPPO is shown in Fig. 8. Comparisons in four trapezoid layers of 300–374, 374–477, 477–596 and 596–753 hPa are illustrated (data above 300 hPa were not shown due to lack of in situ aircraft measurement). Overall, the correlation between the IASI retrievals and the aircraft measurements is very good (0.80 ~ 0.89), but IASI retrievals have a lower bias between −0.69 and −1.74 % as compared to in-situ aircraft measurements (convolved), and the residual standard deviations are between 1.07 and 1.25 %. From Fig. 8 we cannot see significant difference of the errors among different campaigns of HIPPO, which were taken in different seasons, however, on average the bias from HIPPO-1 is the largest, particularly in the high Northern Hemisphere. We found this large bias is associated with the small DOF during the cold winter in the Arctic region.

The mean bias and RMS error of the retrieval in 100 levels are shown in Fig. 9. For comparison the error of the first-guess profile is also plotted. A larger negative bias occurs between 300–500 hPa, and below 500 hPa, both the bias and rms errors are smaller than the first-guess error. As expected, the errors of the convolved data are smaller than that without applying the averaging kernels (Xiong et al., 2008). A larger retrieval bias than the first-guess bias indicates some uncertainty in the empirical bias correction to the radiance, which was pre-computed as the difference of AIRS observed radiance minus the RTA computation using night ocean cases and with the most knowledge of atmospheric profiles and surface emissivity, and needs to be improved in the

AMTD
6, 2501–2531, 2013

future version. Of course, the error from the extrapolation of the aircraft measurements from its ceiling to the top of atmosphere cannot be ignored, and, if possible, to use a model data in the same day can help to reduce this error. Some error results from the time difference between the the measurement of Metrop-A (usually 9.30 a.m. and 9.30 p.m.) and aircraft measurement, however, CH_4 is a well mixed greenhouse gases and this error is expected to be small.

Examination the retrieval error (IASI – convolved in situ) in different latitudes (upper left) of Fig. 10 shows that the retrieval error in the high northern latitudes is slightly larger than in the tropics and the Southern Hemisphere. To better understand the error sources, we examined the correlation of the retrievals with a couple of parameters. We found the results for the four trapezoids in Fig. 8 are similar, so only the results at the trapezoid 374–477 hPa are shown in Fig. 10. There are some correlation between the retrieval error with the degree of freedom (R = 0.36, upper right of Fig. 10), and if we used the non-convolved aircraft data, i.e. the error (IASI – in situ), the correlation coefficient R is 0.51. This indicates that the convolution procedure using the averaging kernels removes the dependence of the error with the information content and some first-guess bias from the matchup (McMillian et al., 2011). There is a slight negative correlation between the retrieval error with cloud cover fraction (R = −0.26), indicating the impact of cloud-contamination on the retrieval. The correlation between the cloud fraction and the degree of freedom is large (R = −0.63), thus as the scene becomes more cloudy, the IASI CH_4 retrieval sees less of the variation of CH_4 and the DOF decreases.

5 Discussion and Summary

As an operational product in NOAA CLASS system, CH_4 profiles have been retrieved using IASI data since 2008. To help users to utilize this product appropriately, this paper provided the first validation of NOAA CH_4 product from IASI retrievals using 596 profiles

AMTD
6, 2501–2531, 2013

from all five campaigns of the HIPPO aircraft measurements. The recommended setting of quality flags is also given.

Overall, the degree of freedom of the IASI CH_4 retrieval is less than 1.5, and the information content in the tropics and higher than in high latitude regions. The most sensitivity of this product is between 100–600 hPa in the tropics, 200–750 hPa in the mid to high latitude. Validation using HIPPO aircraft measurements showed that a large bias at 300–500 hPa of nearly −1.74 % at layer 374–477 hPa. The error is larger in the high northern latitude regions and/or cloudy conditions.

The reasons for this negative bias might be due to the uncertainty in the spectroscopy near methane Q-branch and errors in the RTA, cloud-contamination in the cloud-cleared radiances, and/or the empirical bias correction. Empirical bias correction will be recomputed using HIPPO and other aircraft measurement data to remove this bias in the next version of the IASI retrieval algorithm.

This algorithm is being used by NOAA/NESDIS to exploit Cross-track Infrared Sounder (CrIS) to generate CH_4 and other carbon products routinely at NOAA. Use of the 2nd IASI instrument on Metop-B, which was successfully launched on 17 September 2012, will ensure continuity of the IASI product in the future. A combination of AIRS, IASI and CrIS will enable us to achieve 20+ years' data, which, as a supplementary data to current observations from ground-based network and aircraft measurements, will help us to obtain 3-D distribution of CH_4 with a better spatial coverage and better understand the CH_4 emission and transport in the Arctic.

Ongoing research will focus on optimizing the CH_4 retrieval algorithm to generate a consistent product from these three sensors. Further validation/comparison using other satellites (e.g. GOSAT, TES) and in-situ ground-based and aircraft measurements will be necessary. Comparison of NOAA IASI product with the EUMETSAT product will be helpful, however, differences between NOAA and EUMETSAT products can be due to the difference in the retrieval method, use of the a-priori, radiative transfer model and the input temperature-water vapor profiles. This will be a topic of future research. We also plan to work with modelers to assimilate these TIR CH_4 observation into models

AMTD
6, 2501–2531, 2013

to better quantify the CH_4 source and sinks, however, there is much work to be done to properly utilize these data in data assimilation.

Acknowledgements. This research was supported by funding from NOAA Product System Development and Implementation (PSDI) program. The views, opinions, and findings contained in this paper are those of the authors and should not be construed as an official National Oceanic and Atmospheric Administration or US Government position, policy, or decision.

References

Aumann, H. H., Chahine, M. T., Gautier, C., Goldberg, M. D., Kalnay, E., McMillin, L. M., Revercomb, H., Rosenkranz, P. W., Smith, W. L., Staelin, D. H., Strow, L. L., and Susskind, J.: AIRS/AMSU/HSB on the aqua mission: design, science objectives, data products, and processing systems, IEEE T. Geosci. Remote, 41, 253–264, 2003.

Biastoch, A., Treude, T., Rüpke, L. H., Riebesell, U., Roth, C., Burwicz, E. B., Park, W., Latif, M., Böning, C. W., Madec, G., and Wallmann, K.: rising arctic ocean temperatures cause gas hydrate destabilization and ocean acidification, Geophys. Res. Lett., 38, L08602, doi:10.1029/2011gl047222, 2011.

Bousquet, P., Ciais, P., Miller, J. B., Dlugokencky, E. J., Hauglustaine, D. A., Prigent, C., van der Werf, G. R., Peylin, P., Brunke, E. G., Carouge, C., Langenfelds, R. L., Lathière, J., Papa, F., Ramonet, M., Schmidt, M., Steele, L. P., Tyler, S. C., and White, J.: Contribution of anthropogenic and natural sources to atmospheric methane variability, Nature, 443, 439–443, doi:10.1038/nature05132, 2006.

Bousquet, P., Ringeval, B., Pison, I., Dlugokencky, E. J., Brunke, E.-G., Carouge, C., Chevallier, F., Fortems-Cheiney, A., Frankenberg, C., Hauglustaine, D. A., Krummel, P. B., Langenfelds, R. L., Ramonet, M., Schmidt, M., Steele, L. P., Szopa, S., Yver, C., Viovy, N., and Ciais, P.: Source attribution of the changes in atmospheric methane for 2006–2008, Atmos. Chem. Phys., 11, 3689–3700, doi:10.5194/acp-11-3689-2011, 2011.

Brasseur, G. P., Hauglustaine, D. A., Walters, S., Rasch, P. J., Müller, J. F., Granier, C., and Tie, X. X.: MOZART, a global chemical transport model for ozone and related chemical tracers 1. model description, J. Geophys. Res., 103, 28265–28290, doi:10.1029/98jd02397, 1998.

AMTD
6, 2501–2531, 2013

Chen, Y.-H. and Prinn, R. G.: Estimation of atmospheric methane emissions between 1996 and 2001 using a three-dimensional global chemical transport model, J. Geophys. Res., 111, D10307, doi:10.1029/2005jd006058, 2006.

Clerbaux, C., Hadji-Lazaro, J., Turquety, S., Mégie, G., and Coheur, P.-F.: Trace gas measurements from infrared satellite for chemistry and climate applications, Atmos. Chem. Phys., 3, 1495–1508, doi:10.5194/acp-3-1495-2003, 2003.

Crevoisier, C., Nobileau, D., Fiore, A. M., Armante, R., Chédin, A., and Scott, N. A.: Tropospheric methane in the tropics – first year from IASI hyperspectral infrared observations, Atmos. Chem. Phys., 9, 6337–6350, doi:10.5194/acp-9-6337-2009, 2009.

De Mazière, M., Vigouroux, C., Bernath, P. F., Baron, P., Blumenstock, T., Boone, C., Brogniez, C., Catoire, V., Coffey, M., Duchatelet, P., Griffith, D., Hannigan, J., Kasai, Y., Kramer, I., Jones, N., Mahieu, E., Manney, G. L., Piccolo, C., Randall, C., Robert, C., Senten, C., Strong, K., Taylor, J., Tétard, C., Walker, K. A., and Wood, S.: Validation of ACE-FTS v2.2 methane profiles from the upper troposphere to the lower mesosphere, Atmos. Chem. Phys., 8, 2421–2435, doi:10.5194/acp-8-2421-2008, 2008.

Dlugokencky, E. J., Houweling, S., Bruhwiler, L., Masarie, K. A., Lang, P. M., Miller, J. B., and Tans, P. P.: Atmospheric methane levels off: Temporary pause or a new steady-state?, Geophys. Res. Lett., 30, 1992, doi:10.1029/2003gl018126, 2003.

Dlugokencky, E. J., Myers, R. C., Lang, P. M., Masarie, K. A., Crotwell, A. M., Thoning, K. W., Hall, B. D., Elkins, J. W., and Steele, L. P.: Conversion of NOAA atmospheric dry air CH_4 mole fractions to a gravimetrically prepared standard scale, J. Geophys. Res., 110, D18306, doi:10.1029/2005JD006035, 2005.

Dlugokencky, E. J., Bruhwiler, L., White, J. W. C., Emmons, L. K., Novelli, P. C., Montzka, S. A., Masarie, K. A., Lang, P. M., Crotwell, A. M., Miller, J. B., and Gatti, L. V.: Observational constraints on recent increases in the atmospheric CH_4 burden, Geophys. Res. Lett., 36, L18803, doi:10.1029/2009gl039780, 2009.

Frankenberg, C., Bergamaschi, P., Butz, A., Houweling, S., Meirink, J. F., Notholt, J., Petersen, A. K., Schrijver, H., Warneke, T., and Aben, I.: Tropical methane emissions: A revised view from SCIAMACHY onboard ENVISAT, Geophys. Res. Lett., 35, D04302, doi:10.1029/2008gl034300, 2008.

AMTD
6, 2501–2531, 2013

Frankenberg, C., Aben, I., Bergamaschi, P., Dlugokencky, E. J., van Hees, R., Houweling, S., van der Meer, P., Snel, R., and Tol, P.: Global column-averaged methane mixing ratios from 2003 to 2009 as derived from SCIAMACHY: Trends and variability, J. Geophys. Res., 116, L15811, doi:10.1029/2010jd014849, 2011.

Kort, E. A., Wofsy, S. C., Daube, B. C., Diao, M., Elkins, J. W., Gao, R. S., Hintsa, E. J., Hurst, D. F., Jimenez, R., Moore, F. L., Spackman, J. R., and Zondlo, M. A.: Atmospheric observations of Arctic Ocean methane emissions up to 82° north, Nat. Geosci., 5, 318–321, doi:10.1038/ngeo1452, 2012.

MacDougall, A. H., Avis, C. A., and Weaver, A. J.: Significant contribution to climate warming from the permafrost carbon feedback, Nat. Geosci., 5, 719–721, doi:10.1038/ngeo1573, 2012.

Maddy, E. S. and Barnet, C. D.: Vertical resolution estimates in version 5 of AIRS operational retrievals, IEEE T. Geosci. Remote, 46, 2375–2384, doi:10.1109/tgrs.2008.917498, 2008.

Maddy, E. S., Barnet, C. D., and Gambacorta, A.: A computationally efficient retrieval algorithm for hyperspectral sounders incorporating a priori information, IEEE Geosci. Remote S., 6, 802–806, doi:10.1109/lgrs.2009.2025780, 2009.

Maddy, E. S., King, T. S., Sun, H., Wolf, W. W., Barnet, C. D., Heidinger, A., Cheng, Z., Goldberg, M. D., Gambacorta, A., Zhang, C., and Zhang, K.: Using MetOp-AAVHRR clear-sky measurements to Cloud-ClearMetOp-AIASI column radiances, J. Atmos. Ocean. Tech., 28, 1104–1116, doi:10.1175/jtech-d-10-05045.1, 2011.

Maddy, E. S., DeSouza-Machado, S. G., Nalli, N. R., Barnet, C. D. L., Strow, L., Wolf, W. W., Xie, H., Gambacorta, A., King, T. S., Joseph, E., Morris, V., Hannon, S. E., and Schou, P.: On the effect of dust aerosols on AIRS and IASI operational level 2 products, Geophys. Res. Lett., 39, L10809, doi:10.1029/2012gl052070, 2012.

McMillan, W. W., Evans, K. D., Barnet, C. D., Maddy, E. S., Sachse, G. W., and Diskin, G. S.: Validating the AIRS version 5 CO retrieval with DACOM in situ measurements during INTEX-A and -B, IEEE T. Geosci. Remote, 49, 2802–2813, doi:10.1109/tgrs.2011.2106505, 2011.

Park, M., Randel, W. J., Kinnison, D. E., Garcia, R. R., and Choi, W.: Seasonal variation of methane, water vapor, and nitrogen oxides near the tropopause: Satellite observations and model simulations, J. Geophys. Res., 109, D03302, doi:10.1029/2003jd003706, 2004.

Patra, P. K., Houweling, S., Krol, M., Bousquet, P., Belikov, D., Bergmann, D., Bian, H., Cameron-Smith, P., Chipperfield, M. P., Corbin, K., Fortems-Cheiney, A., Fraser, A., Gloor, E., Hess, P., Ito, A., Kawa, S. R., Law, R. M., Loh, Z., Maksyutov, S., Meng, L., Palmer, P. I.,

AMTD
6, 2501–2531, 2013

Prinn, R. G., Rigby, M., Saito, R., and Wilson, C.: TransCom model simulations of CH_4 and related species: linking transport, surface flux and chemical loss with CH_4 variability in the troposphere and lower stratosphere, Atmos. Chem. Phys., 11, 12813–12837, doi:10.5194/acp-11-12813-2011, 2011.

Payan, S., Camy-Peyret, C., Oelhaf, H., Wetzel, G., Maucher, G., Keim, C., Pirre, M., Huret, N., Engel, A., Volk, M. C., Kuellmann, H., Kuttippurath, J., Cortesi, U., Bianchini, G., Mencaraglia, F., Raspollini, P., Redaelli, G., Vigouroux, C., De Mazière, M., Mikuteit, S., Blumenstock, T., Velazco, V., Notholt, J., Mahieu, E., Duchatelet, P., Smale, D., Wood, S., Jones, N., Piccolo, C., Payne, V., Bracher, A., Glatthor, N., Stiller, G., Grunow, K., Jeseck, P., Te, Y., and Butz, A.: Validation of version-4.61 methane and nitrous oxide observed by MIPAS, Atmos. Chem. Phys., 9, 413–442, doi:10.5194/acp-9-413-2009, 2009.

Payne, V. H., Clough, S. A., Shephard, M. W., Nassar, R., and Logan, J. A.: Information-centered representation of retrievals with limited degrees of freedom for signal: application to methane from the Tropospheric Emission Spectrometer, J. Geophys. Res., 114, D10307, doi:10.1029/2008jd010155, 2009.

Razavi, A., Clerbaux, C., Wespes, C., Clarisse, L., Hurtmans, D., Payan, S., Camy-Peyret, C., and Coheur, P. F.: Characterization of methane retrievals from the IASI space-borne sounder, Atmos. Chem. Phys., 9, 7889–7899, doi:10.5194/acp-9-7889-2009, 2009.

Rigby, M., Prinn, R. G., Fraser, P. J., Simmonds, P. G., Langenfelds, R. L., Huang, J., Cunnold, D. M., Steele, L. P., Krummel, P. B., Weiss, R. F., O'Doherty, S., Salameh, P. K., Wang, H. J., Harth, C. M., Mühle, J., and Porter, L. W.: Renewed growth of atmospheric methane, Geophys. Res. Lett., 35, L22805, doi:10.1029/2008gl036037, 2008.

Rodgers, C. D.: Inverse Methods for Atmospheric Sounding: Theory and Practice, University of Oxford, World Sci., River Edge, NJ, USA, 2000.

Schepers, D., Guerlet, S., Butz, A., Landgraf, J., Frankenberg, C., Hasekamp, O., Blavier, J. F., Deutscher, N. M., Griffith, D. W. T., Hase, F., Kyro, E., Morino, I., Sherlock, V., Sussmann, R., and Aben, I.: Methane retrievals from greenhouse gases observing satellite (GOSAT) shortwave infrared measurements: performance comparison of proxy and physics retrieval algorithms, J. Geophys. Res., 117, D10307, doi:10.1029/2012jd017549, 2012.

Shakhova, N., Semiletov, I., Salyuk, A., Yusupov, V., Kosmach, D., and Gustafsson, O.: Extensive methane venting to the atmosphere from sediments of the East Siberian arctic shelf, Science, 327, 1246, doi:10.1126/science.1182221, 2010.

AMTD
6, 2501–2531, 2013

Shakhova, N. E., Semiletov, I. P., Salyuk, A., Stubbs, C., Kosmach, D., and Gustafsson, O.: Ebullition-driven fluxes of methane from shallow hot spots suggest significant underestimation of annual emission from the East Siberian Arctic Shelf, American Geophysical Union, Fall Meeting 2011, abstract #GC41B-0794, San Francisco, CA, 2011.

Shindell, D. T., Walter, B. P., and Faluvegi, G.: Impacts of climate change on methane emissions from wetlands, Geophys. Res. Lett., 31, L21202, doi:10.1029/2004gl021009, 2004.

Simpson, I. J., Chen, T.-Y., Blake, D. R., and Rowland, F. S.: Implications of the recent fluctuations in the growth rate of tropospheric methane, Geophys. Res. Lett., 29, 117–111, doi:10.1029/2001gl014521, 2002.

Solomon, S.: IPCC (2007): Climate Change The Physical Science Basis, American Geophysical Union, Fall Meeting 2007, abstract #U43D-01, San Francisco, CA, 2007.

Strow, L. L., Hannon, S. E., De Souza-Machado, S., Motteler, H. E., and Tobin, D.: An overview of the AIRS radiative transfer model, IEEE T. Geosci. Remote, 41, 303–313, 2003.

Susskind, J., Barnet, C. D., and Blaisdell, J. M.: Retrieval of atmospheric and surface parameters from AIRS/AMSU/HSB data in the presence of clouds, IEEE T. Geosci. Remote, 41, 390–409, doi:10.1109/tgrs.2002.808236, 2003.

Sussmann, R., Forster, F., Rettinger, M., and Bousquet, P.: Renewed methane increase for five years (2007–2011) observed by solar FTIR spectrometry, Atmos. Chem. Phys., 12, 4885–4891, doi:10.5194/acp-12-4885-2012, 2012.

Walter, K. M., Zimov, S. A., Chanton, J. P., Verbyla, D., and Chapin, F. S.: Methane bubbling from Siberian thaw lakes as a positive feedback to climate warming, Nature, 443, 71–75, doi:10.1038/nature05040, 2006.

Wecht, K. J., Jacob, D. J., Wofsy, S. C., Kort, E. A., Worden, J. R., Kulawik, S. S., Henze, D. K., Kopacz, M., and Payne, V. H.: Validation of TES methane with HIPPO aircraft observations: implications for inverse modeling of methane sources, Atmos. Chem. Phys., 12, 1823–1832, doi:10.5194/acp-12-1823-2012, 2012.

Wofsy, S. C. and Hippo Science Team: HIAPER Pole-to-Pole Observations (HIPPO): Global distributions and emission sources for CH_4, N_2O, Black Carbon, and other trace species inferred from five aircraft missions, American Geophysical Union, Fall Meeting 2011, abstract #A13J-02, San Francisco, CA, 2011.

AMTD
6, 2501–2531, 2013

Worden, J., Kulawik, S., Frankenberg, C., Payne, V., Bowman, K., Cady-Peirara, K., Wecht, K., Lee, J.-E., and Noone, D.: Profiles of CH_4, HDO, H_2O, and N_2O with improved lower tropospheric vertical resolution from Aura TES radiances, Atmos. Meas. Tech., 5, 397–411, doi:10.5194/amt-5-397-2012, 2012.

Xiong, X., Barnet, C., Maddy, E., Sweeney, C., Liu, X., Zhou, L., and Goldberg, M.: Characterization and validation of methane products from the Atmospheric Infrared Sounder (AIRS), J. Geophys. Res., 113, G00A01, doi:10.1029/2007jg000500, 2008.

Xiong, X., Houweling, S., Wei, J., Maddy, E., Sun, F., and Barnet, C.: Methane plume over south Asia during the monsoon season: satellite observation and model simulation, Atmos. Chem. Phys., 9, 783–794, doi:10.5194/acp-9-783-2009, 2009.

Xiong, X., Barnet, C., Maddy, E., Wei, J., Liu, X., and Pagano, T. S.: Seven years' observation of mid-upper tropospheric methane from atmospheric infrared sounder, Remote Sens., 2, 2509–2530, doi:10.3390/rs2112509, 2010a.

Xiong, X., Barnet, C. D., Zhuang, Q., Machida, T., Sweeney, C., and Patra, P. K.: Mid-upper tropospheric methane in the high Northern Hemisphere: Spaceborne observations by AIRS, aircraft measurements, and model simulations, J. Geophys. Res., 115, D19309, doi:10.1029/2009JD013796, 2010b.

Yokota, T., Watanabe, H., Uchino, O., Morino, I., Yoshida, Y., and Maksyutov, S.: Current status of the GOSAT data handling facility, data retrieval and inverse model algorithms, validation plan, and GOSAT research announcement, American Geophysical Union, Fall Meeting 2008, abstract #A32B-02, San Francisco, CA, 2008.

Zhuang, Q., Melack, J. M., Zimov, S., Walter, K. M., Butenhoff, C. L., and Khalil, M. A. K.: Global methane emissions from wetlands, rice paddies, and lakes, eos, EOS T. Am. Geophys. Un., 90, 37–38, doi:10.1029/2009eo050001, 2009.

Zimov, S. A., Davydov, S. P., Zimova, G. M., Davydova, A. I., Schuur, E. A. G., Dutta, K., and Chapin, F. S.: Permafrost carbon: Stock and decomposability of a globally significant carbon pool, Geophys. Res. Lett., 33, L20502, doi:10.1029/2006gl027484, 2006.

AMTD
6, 2501–2531, 2013

Table 1. IASI trapezoid layers in retrieval (hPa).

Level	1	2	3	4	5	6	7	8	9	10	11	12
hPa	0.016	11.0	96.1	151.3	223.4	300.0	374.7	478.0	596.3	753.6	904.8	1100.0

AMTD
6, 2501–2531, 2013

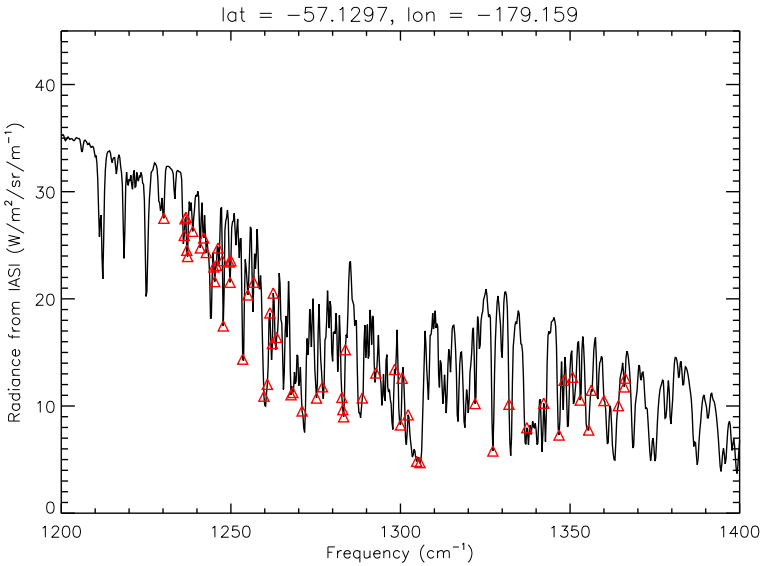

Fig. 1. An example of IASI observed radiance near the 7.66 micron CH_4 absorption band at the location (57.1297° S, 179.159° W) on 15 September 2009. Red triangles marks the channels used in the NOAA IASI retrieval system.

AMTD
6, 2501–2531, 2013

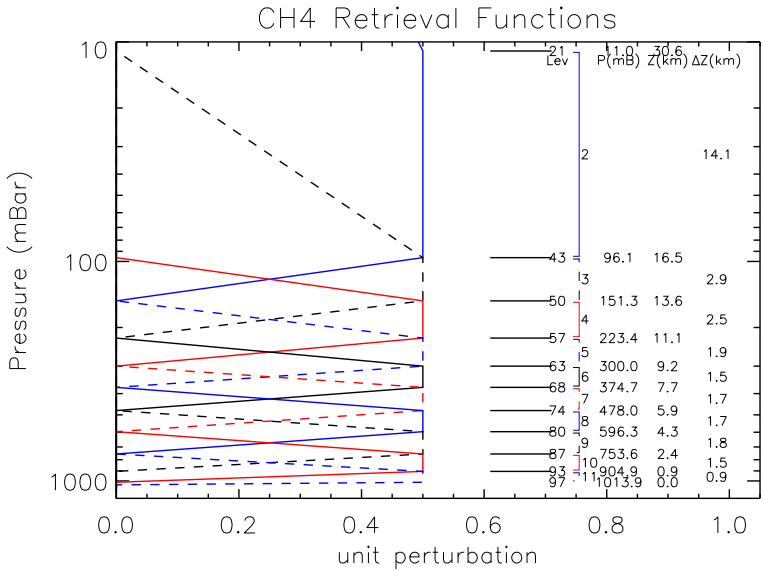

Fig. 2. The eleven trapezoidal perturbation functions for the IASI CH_4 retrieval. Lev is the level number in 100 levels grid of Radiative Transfer Algorithm (RTA) (Strow et al., 2003).

AMTD
6, 2501–2531, 2013

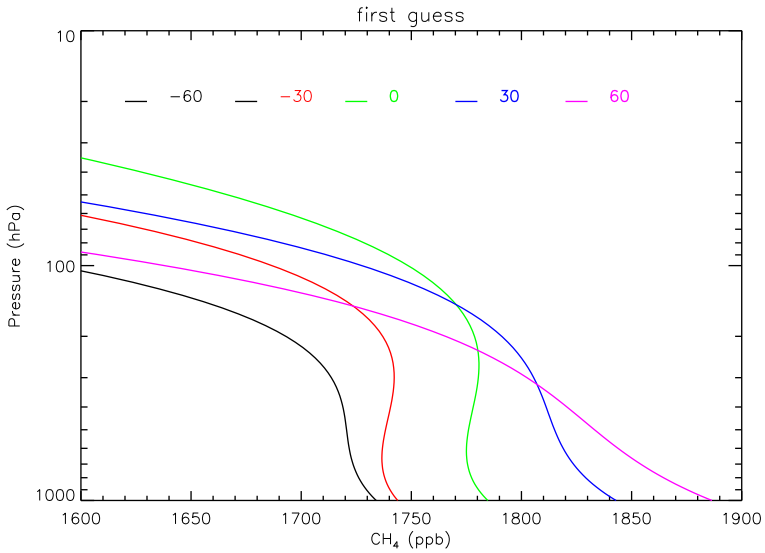

Fig. 3. Example of the first-guess profiles in latitudes of 60° S, 30° S, 0, 30° N and 60° N.

AMTD
6, 2501–2531, 2013

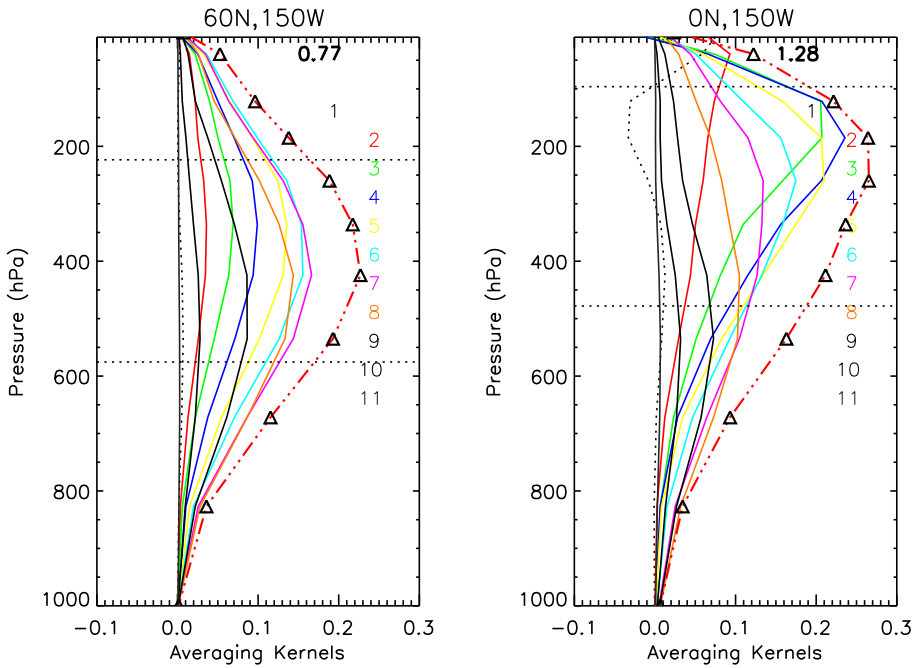

Fig. 4. The averaging kernels in high Northern Hemisphere and tropics over the Pacific Ocean in September 2009. Different colors correspond to 11 different trapozoid functions (see Table 1). In order to plot the area of the averaging kernels in the same range of x-axis, the red dash line is the area of averaging kernels divided by 4.

AMTD
6, 2501–2531, 2013

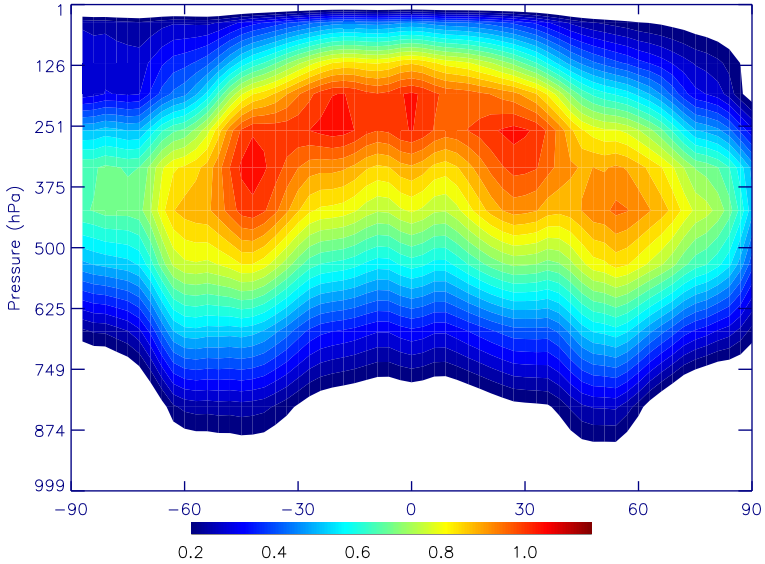

Fig. 5. The zonal mean of the area of averaging kernels in different latitude. x-axis is the latitude. Color bar represents the value of the area of averaging kernels (no unit).

AMTD
6, 2501–2531, 2013

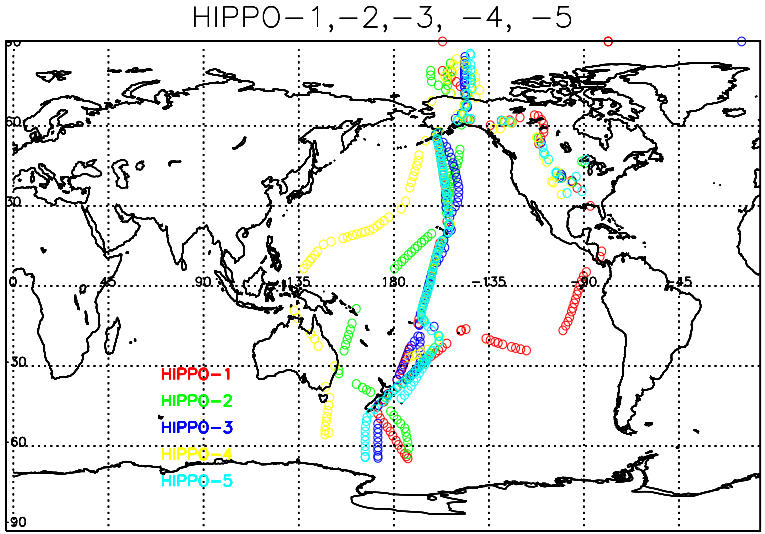

Fig. 6. locations and numbers of aircraft measurement profiles selected for validation from HIPPO-1 (red, N = 121), HIPPO-2 (green, N = 121), HIPPO-3 (blue, N = 88), HIPPO-4 (yellow, N = 121) and HIPPO-5 (cryn, N = 145).

AMTD
6, 2501–2531, 2013

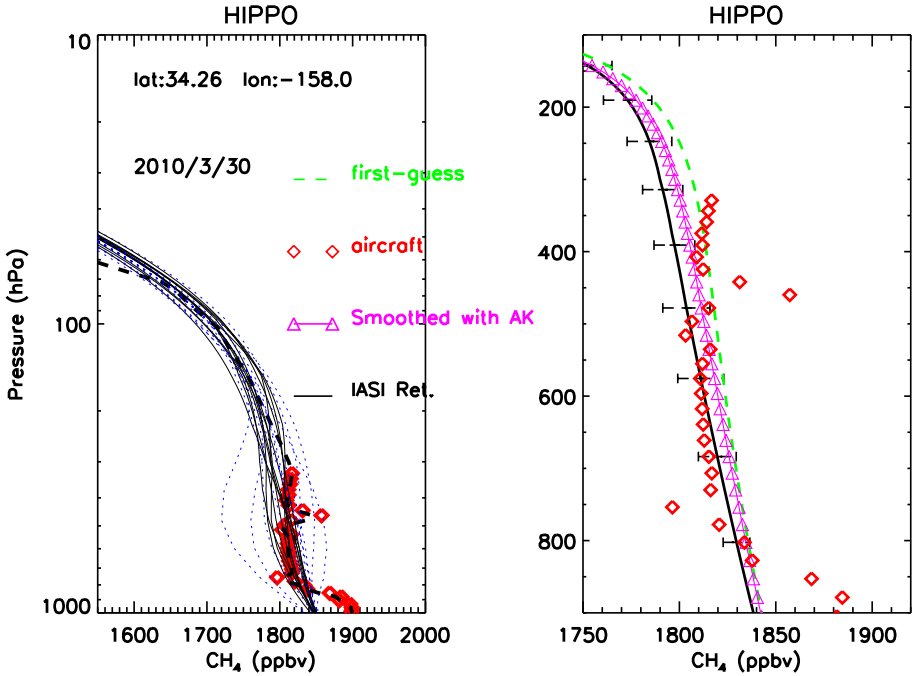

Fig. 7. CH_4 profile on 30 March 2010 by HIPPO-3 aircraft measurement (red dots) vs all IASI retrievals in a collocation window with a distance of 100 km and in the same day. Blue dash lines are profiles that fail to pass the criteria of quality control. The right panel is the mean profile of IASI retrievals with the bars showing the standard deviation, the aircraft measurements smoothed with the averaging kernels (AK) (puple, triangles), and the first guess profile (green dash line).

AMTD
6, 2501–2531, 2013

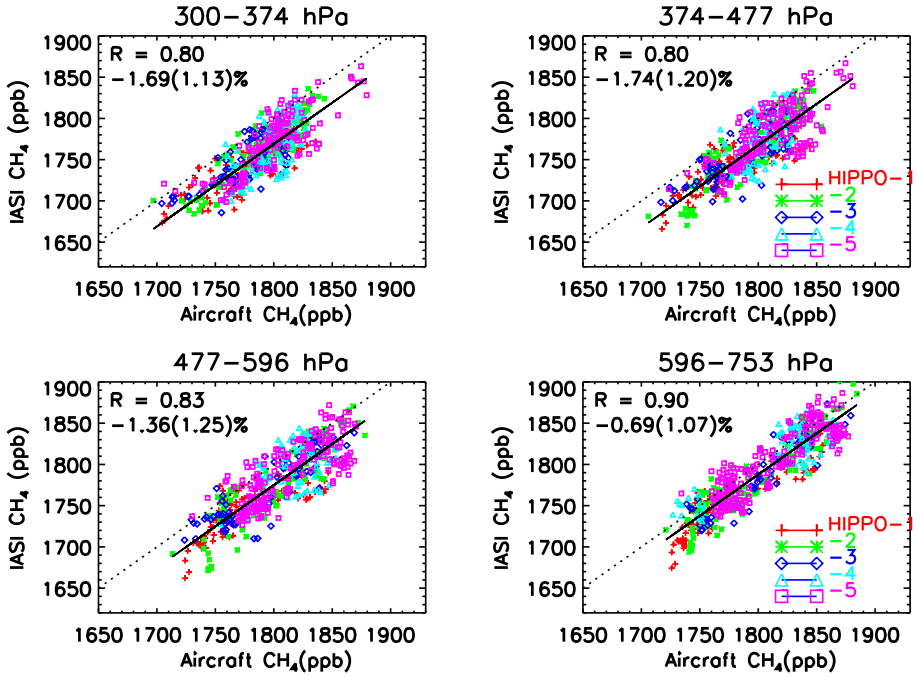

Fig. 8. IASI retrieved CH_4 mixing ratio with aircraft profiles from HIPPO-1, -2, -3, -4 and -5 in four trapezoid layers of 300–374, 374–477, 477–596 and 596–753 hPa. x-axis is the convolved aircraft measurements, and y-axis is the mean of IASI retrieved profiles within 200 km and in the same day of the measurement time and site location. Different colors are from different campaigns of HIPPO. *R* is the correlation coefficient, and below it is the bias and residual standard deviation in percentage (%).

AMTD
6, 2501–2531, 2013

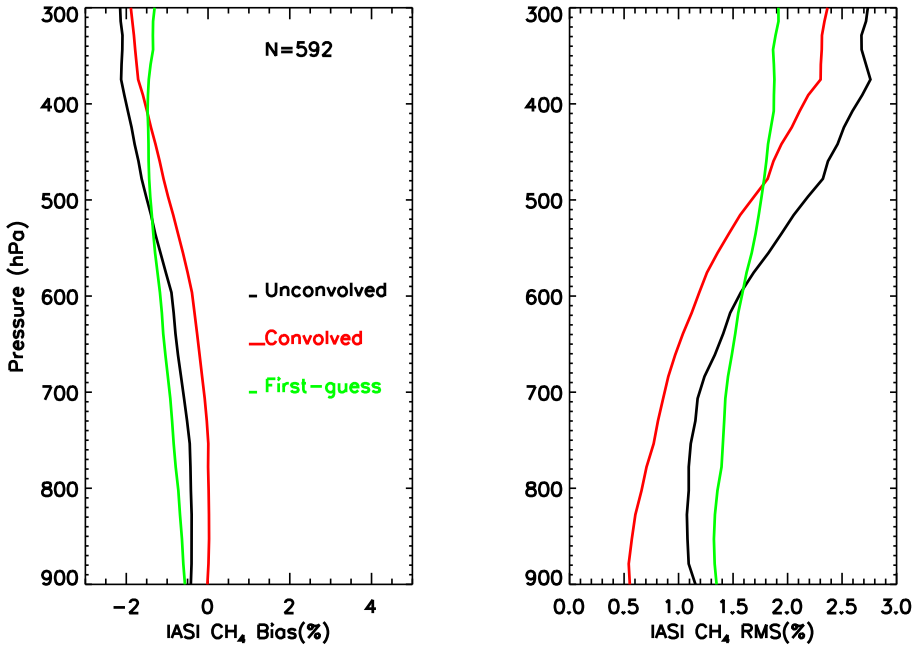

Fig. 9. Bias (left) and RMS errors (right) of the IASI retrieved CH_4 mixing ratio and the first guess profile as compared to aircraft profiles from HIPPO.

AMTD
6, 2501–2531, 2013

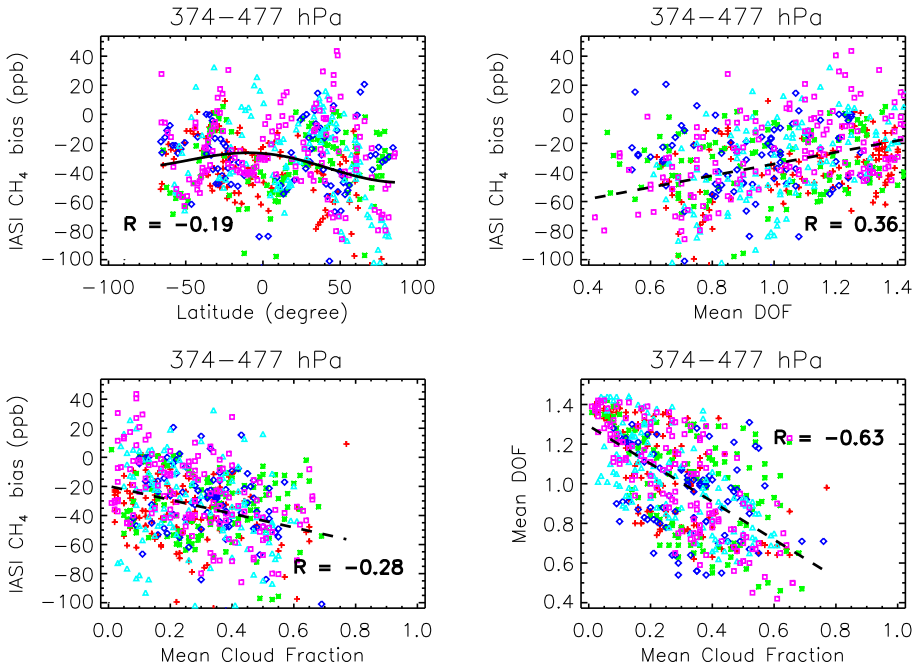

Fig. 10. Correlations of the IASI CH_4 retrieval bias in layer 374–477 hPa with latitude (the solid line is the 2nd order polynomial fitting of the error with latitude), and the correlation between the IASI CH_4 retrieval bias with mean degree of freedom (DOF) and cloud fraction, and the correlation between the mean degree of freedom (DOF) and cloud fraction. Similar results are found for other trapezoids. Different colors are for different campaigns as defined in Fig. 8.

AMTD
6, 2501–2531, 2013